PLOS GENETICS

RESEARCH ARTICLE

3 minutes to precisely measure morphogen concentration

Tanguy Lucas[1☯], **Huy Tran**[1,2☯], **Carmina Angelica Perez Romero**[1,3], **Aurélien Guillou**[1], **Cécile Fradin**[1,3], **Mathieu Coppey**[4], **Aleksandra M. Walczak**[2], **Nathalie Dostatni**[1*]

1 Institut Curie, PSL Research University, CNRS, Sorbonne Université, Nuclear Dynamics, Paris, France, **2** Ecole Normale Supérieure, PSL Research University, CNRS, Sorbonne Université, Physique Théorique, Paris, France, **3** Dept. of Physics and Astronomy, McMaster University, Hamilton, Ontario, Canada, **4** Institut Curie, PSL Research University, CNRS, Sorbonne Université, Physico Chimie, Paris, France

☯ These authors contributed equally to this work.
* nathalie.dostatni@curie.fr

Citation: Lucas T, Tran H, Perez Romero CA, Guillou A, Fradin C, Coppey M, et al. (2018) 3 minutes to precisely measure morphogen concentration. PLoS Genet 14(10): e1007676. https://doi.org/10.1371/journal.pgen.1007676

Editor: Michael B. Eisen, University of California Berkeley, UNITED STATES

Received: April 26, 2018

Accepted: September 5, 2018

Published: October 26, 2018

Data Availability Statement: RNA FISH data and the time lapse movies are accessible at the following link: http://xfer.curie.fr/get/NjnfH8faAlt/LUCAS_2018_DATA.zip in the form of a Zipped folder of ~ 50 Go. All other relevant data are within the paper and its Supporting Information files.

Funding: This work was supported by a PSL IDEX REFLEX Grant for Mesoscopic Biology (ND, AMW, MC), ANR- 11-BSV2-0024 Axomorph (ND and AMW), ARC PJA20151203341 (ND), ANR-11-LABX-0044 DEEP Labex (ND), an Ontario Trillium Scholarship for International Students (CAPR), a

Abstract

Morphogen gradients provide concentration-dependent positional information along polarity axes. Although the dynamics of the establishment of these gradients is well described, precision and noise in the downstream activation processes remain elusive. A simple paradigm to address these questions is the Bicoid morphogen gradient that elicits a rapid step-like transcriptional response in young fruit fly embryos. Focusing on the expression of the major Bicoid target, *hunchback* (*hb*), at the onset of zygotic transcription, we used the MS2-MCP approach which combines fluorescent labeling of nascent mRNA with live imaging at high spatial and temporal resolution. Removing 36 putative Zelda binding sites unexpectedly present in the original MS2 reporter, we show that the 750 bp of the *hb* promoter are sufficient to recapitulate endogenous expression at the onset of zygotic transcription. After each mitosis, in the anterior, expression is turned on to rapidly reach a plateau with all nuclei expressing the reporter. Consistent with a Bicoid dose-dependent activation process, the time period required to reach the plateau increases with the distance to the anterior pole. Despite the challenge imposed by frequent mitoses and high nuclei-to-nuclei variability in transcription kinetics, it only takes 3 minutes at each interphase for the MS2 reporter loci to distinguish subtle differences in Bicoid concentration and establish a steadily positioned and steep (Hill coefficient ~ 7) expression boundary. Modeling based on the cooperativity between the 6 known Bicoid binding sites in the *hb* promoter region, assuming rate limiting concentrations of the Bicoid transcription factor at the boundary, is able to capture the observed dynamics of pattern establishment but not the steepness of the boundary. This suggests that a simple model based only on the cooperative binding of Bicoid is not sufficient to describe the spatiotemporal dynamics of early *hb* expression.

Mitacs Global Link Scholarship (CAPR) and an Internal Curie Institute Scholarship (CAPR), a Mayent Rothschild sabbatical Grant from the Curie Institute (CF) and an NSERC discovery grant RGPIN/06362-15 (CF), a Marie Curie MCCIG grant No. 303561 (AMW) and PSL ANR-10-IDEX-0001-02. - https://www.psl.eu/en/research/funding-opportunities/psl-calls-proposals - http://www.agence-nationale-recherche.fr/en/ - https://www.fondation-arc.org/espace-chercheur - https://grad.uwo.ca/current_students/student_finances/ots.html - https://www.mitacs.ca/en/programs/globalink - https://enseignement.curie.fr/en/content/senior-researcher-sabbatical - http://www.nserc-crsng.gc.ca/index_eng.asp -https://ec.europa.eu/research/participants/portal/desktop/en/opportunities/fp7/calls/fp7-people-2013-cig.html
The funders had no role in study design, data collection and analysis, decision to publish, or preparation of the manuscript.

Competing interests: The authors have declared that no competing interests exist.

Author summary

During development, the first thing that an embryo needs to know is the orientation of its body. We study how the head-to-tail axis forms in the fruit fly embryo. To position the axis, the embryo relies on proteins called morphogens broadcasting instructions to other genes, so that cells know, depending on where they are along the axis, what they should become. The concentration of the Bicoid morphogen is much higher in the head of the embryo and lower towards the tail. Bicoid activates *hunchback*, which divides the embryo in two parts. By visualizing this process in real time in living embryos, we see the *hunchback* gene activated very efficiently in the head part, where each nucleus expresses the gene, whereas it is not expressed at all in the tail part. Intriguingly, the boundary separating the two domains is precisely positioned and becomes very steep in no more than three minutes. We use a modeling approach to understand how this is achieved so rapidly. Given the parameters of the system, we find that although our model is able to reproduce the fast dynamics of the process, it fails to reproduce the steepness of the boundary suggesting that a more complex approach is needed to capture the additional mechanisms involved.

Introduction

Morphogens are at the origin of complex axial polarities in many biological systems. In these systems, positional information is proposed to be provided by morphogen concentrations, which allow each cell to measure its position along the embryo's axes and turn on expression of target genes responsible for the determination of its identity. Although the existence of these gradients is now well established [1], the quantitative details of their functioning (i.e. how small differences in morphogen concentrations are precisely and robustly interpreted into a threshold-dependent step-like response) remains largely debated [2].

To address this question, we study the Bicoid morphogen, which specifies cell identity along the antero-posterior (AP) axis of the fruit fly embryo [3]. The Bicoid concentration gradient reaches its maximum value at the anterior pole [4] and is distributed steadily in an exponential gradient along the AP axis after one hour of development [4–6] (Fig 1A). Bicoid is a homeodomain transcription factor that binds DNA. Bicoid binding sites are found in the regulatory sequences of Bicoid target genes and are both necessary [7–9] and sufficient [10–12] for Bicoid-dependent expression. Changes in Bicoid dosage induce a shift of the expression boundary of these genes along the AP axis [9, 13] indicating that Bicoid provides concentration-dependent positional information to the system [14]. In young syncytial embryos (nuclear cycles 9 to 13), the major Bicoid target gene *hunchback* (*hb)* is expressed under Bicoid control in a large domain spanning the anterior half of the embryo [15]. At cycle 14, *hb* is also expressed in a narrow posterior domain [16] and in the parasegment 4 [17] and even later during development in the nervous system [18]. Expression of endogenous *hb* is initiated at two different promoters, the distal promoter P1 and the proximal promoter P2 [19]. P1 is responsible for maternal and late blastoderm expression in parasegment 4 and in the posterior stripe [16, 17]. P2 mediates the early Bcd-dependent expression of *hb* [17, 19]. At nuclear cycle 14, expression of endogenous *hb* is also controlled by two distal enhancers, the shadow enhancer and the stripe enhancer, which both contribute to the robustness of *hb* expression [20, 21].

Here, we focus exclusively on the most early zygotic expression of *hb*, which is Bicoid-dependent, driven by the P2 promoter and occurring from nc11 to nc13. Just 30 min after the onset of zygotic transcription and the steady establishment of the Bicoid gradient, endogenous

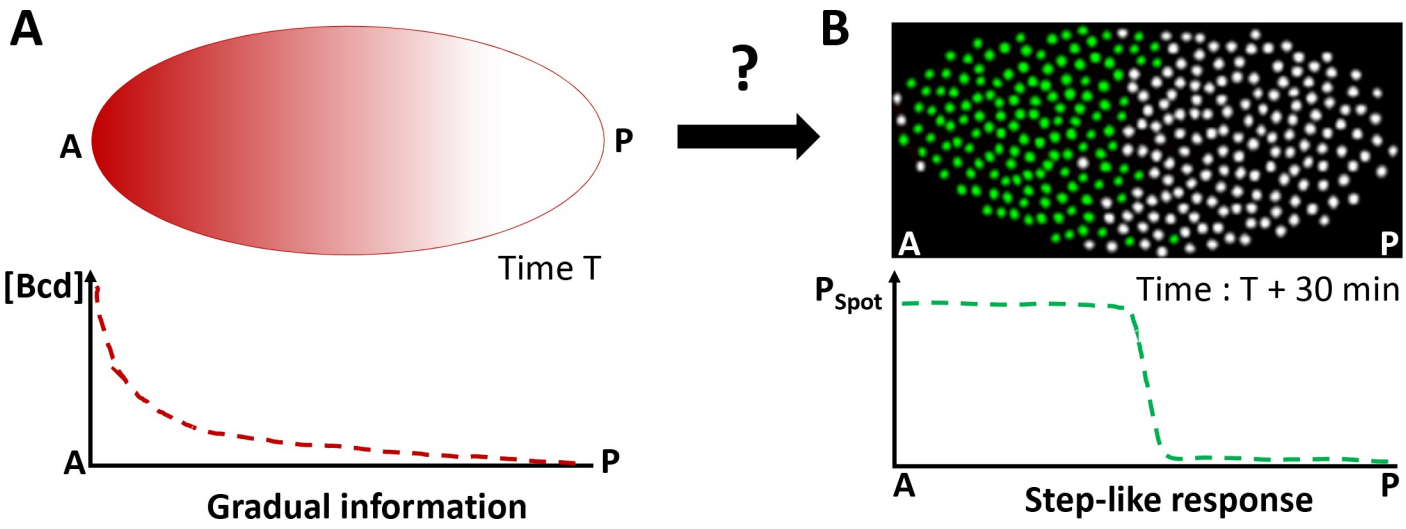

Fig 1. The Bicoid system transforms the gradual information contained in the Bicoid concentration gradient into a step-like response in 30 min. A) At nc 8 (T = 1 hr), the Bicoid exponential gradient (red) is steadily established [5, 6] with its highest concentration at the anterior pole (A) and its lowest concentration at the posterior pole (P). The first hints of zygotic transcription are detected by RNA FISH marking the onset of zygotic transcription [15]. **B)** At nc 11 (T = 1 hr 30 min), the main Bicoid target gene, *hunchback* (*hb*), is expressed within a large anterior expression domain. *hb* expression is schematized here from RNA FISH data [15]: nuclei where ongoing transcription at the *hb* loci is detected are shown in green and nuclei silent for *hb* are shown in white.

https://doi.org/10.1371/journal.pgen.1007676.g001

hb already exhibits a step-like expression pattern [15]. At this developmental time period, this pattern is characterized by an anterior domain containing almost exclusively *hb* transcriptionally active nuclei and a posterior domain containing exclusively *hb* silent nuclei [3] (Fig 1B). The boundary separating expressing and non-expressing nuclei is very steep despite the stochastic nature of transcription in eukaryotic cells [22], the short interphase duration (~5 min) and the subtle difference in the Bicoid concentration (10%) on either side of the boundary [15]. How the *hb* pattern so rapidly acquires such a steep boundary with high levels of expression in the whole anterior domain is unclear. It could involve a purely quantitative threshold-dependent process, in which Bicoid, acting as a direct transcription activator, is the main source of positional information. Alternatively, additional mechanisms including activation by maternal Hb [12, 15, 23] or posterior inhibitors such as those acting later during development at cycle 14 to set the position of the boundary along the AP axis [7, 24, 25] could be considered. In any case, the mechanism involved should account for a Bicoid dose-dependent effect on the positioning of the boundary along the AP axis. Also, given the early timing of development, most actors in this process are likely to be already present at the onset of zygotic transcription and therefore maternally provided.

To shed light on the formation of the *hb* expression boundary during these early steps of development, we have previously adapted the MS2-MCP approach to developing fly embryos [26]. This approach allows the fluorescent tagging of RNA in living cells and provides access to the transcription dynamics of an MS2 reporter locus [27, 28]. In our first attempt, we placed the *hb* P2 proximal promoter region (~ 750 bp) upstream of an MS2 cassette containing 24 MS2 loops and analyzed expression of this reporter (*hb-MS2*) in embryos expressing the MCP-GFP protein maternally [26]. The *hb-MS2* reporter was expressed very early as robustly as endogenous *hb* in the anterior half of the embryo. However, unlike endogenous *hb*, the reporter, which only encompasses the *hb* P2 proximal promoter region (~750 bp), was also expressed in the posterior, though more heterogeneously and more transiently than in the anterior. The different expression of the *hb-MS2* reporter and endogenous *hb* in the posterior suggested that, the 750 bp of the *hb* P2 proximal promoter were not sufficient to recapitulate

the endogenous expression of *hb* at the onset of zygotic transcription. The most obvious interpretation of these discrepancies was that the *hb-MS2* reporter was missing key cis-response elements allowing repression of endogenous *hb* by an unknown repressor in the posterior [26].

Here, we first show that the homogenously distributed Zelda transcription factor is responsible for the expression of the *hb-MS2* reporter in the posterior. BAC recombineering indicated that the MS2 cassette itself mediates Zelda posterior expression and *in silico* analysis reveals the presence of about 36 putative Zelda binding sites in the MS2 cassette. A new reporter (*hb-MS2ΔZelda*), placing the *hb* P2 proximal promoter (~750 bp) upstream of a new MS2 cassette (MS2-ΔZelda), in which those unfortunate Zelda binding sites have been mutated, faithfully recapitulates the early expression of endogenous *hb* observed by RNA FISH [15]. Thus, the *hb* P2 proximal promoter (~750 bp) is sufficient for a robust step-like expression of the reporter. Quantitative analysis of the MS2 time traces of this new reporter reveals a transcription process dividing the anterior of the embryo in a saturating zone with stable features and a limiting zone closer to the boundary, with more variable features. A high probability for the promoter to be ON (P_{ON}) is reached faster in the anterior where the concentration of Bicoid is higher than close to the boundary where Bicoid concentration is lower. In each interphase, full step-like response is established in not more than three minutes, after which the expression boundary is locked at a given position along the AP axis. To understand this observed dynamics, we used a simple model of position readout through the binding/unbinding of a transcription factor to *N* operator sites on the *hb* promoter [29]. The model that best fits the data is able to capture the very fast dynamics of establishment of the boundary. However, high steepness of the experimental pattern (coefficient of the fitted Hill function $N_{Hill} \sim 7$, based on various features of the MS2 time-traces) is not achievable assuming only $N = 6$ Bicoid binding sites, which is the number of known Bicoid binding sites in the canonical *hb* promoter [8]. This indicates that a simple equilibrium model only taking into account a single activator and varying degrees of cooperativity between the binding of several molecules on the *hb* promoter in the reporter, from which a steep *hb* pattern can emerge [29], is not sufficient to capture its activity and fit the data. It suggests that additional mechanisms are required to define the steepness of the boundary.

Results

Zelda induces posterior expression of the *hb-MS2* transgene at early cycles

In our first attempt of using the MS2 system to study the transcriptional response downstream of Bicoid, we placed the *hb* P2 proximal promoter region (~ 750 bp) upstream of a classical MS2 cassette [30]. The reporter (*hb-MS2*) was expressed in the posterior of the embryo and did not recapitulate expression of endogenous *hb* [26]. The Zelda transcription factor is a major regulator of the first wave of zygotic transcription in fruit fly embryos [31] and is involved in the transcriptional regulation of the *hb* gene [32]. To determine how Zelda contributes to the expression of the *hb-MS2* reporter, we analyzed expression of the reporter by live imaging (S1 Movie) and double RNA FISH (using *hunchback* and *MS2* probes, Fig 2A) in embryos expressing various amounts of maternal Zelda. As expected [26], wild-type embryos show high expression of the *hb-MS2* reporter both in the anterior and the posterior domain ([26] and Fig 2B, top panel), with an average of 80% of expressing nuclei dispersed through the posterior domain (Fig 2B, bottom panel). In embryos from *zelda* heterozygous mutant females ($zld^{Mat-/+}$), expression of the *hb-MS2* reporter is reduced by 5 fold in the posterior (with only 15% of active nuclei). In embryos from *zelda* mutant germline clones, completely devoid of Zelda maternal contribution ($zld^{Mat-/-}$), expression boundaries of endogenous *hb* and *hb-MS2* reporter are shifted towards the anterior (Fig 2D). Moreover, posterior expression of the *hb-*

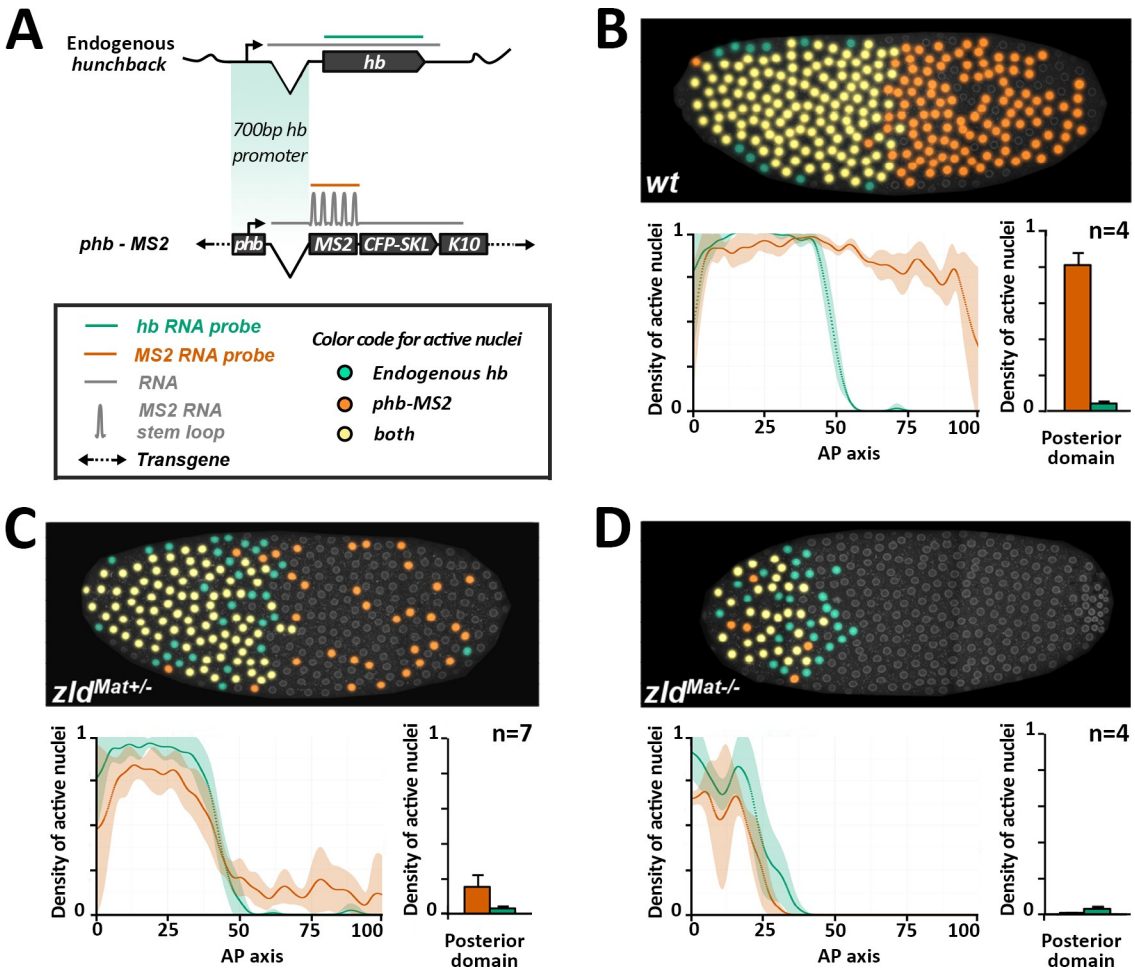

Fig 2. Posterior expression of the *hb-MS2* reporters is Zelda dependent. A) Dual RNA FISH using a *hb* probe (green) and an *MS2* (orange) probe on wild-type embryos carrying one copy of the *hb-MS2* reporter, placing the *MS2-CFP-SKL-K10* cassette under the control of the 750 bp canonical promoter of *hb* [26]. **B-D)** Embryos are wild-type (**B**), from heterozygous mutant females for Zelda (**C**) or germline mutant clones for Zelda (**D**). **Top panels:** Expression map of cycle 11 embryos after segmentation of nuclei and automated processing of FISH staining. Nuclei expressing only *hb* are labelled in green, nuclei expressing only the *hb-MS2* reporter are labelled in orange and nuclei expressing both *hb* and the *hb-MS2* reporter are labelled in yellow. **Bottom panels:** On the left, density of active nuclei for either *hb* (green) or the *hb-MS2* reporter (orange) along the AP axis with the anterior pole on the left (0) and the posterior pole on the right (100). On the right, density of active nuclei for the *hb-MS2* reporter (orange) and *hb* (green) in the posterior domain. For each embryo, the position of the expression boundary is calculated as the position of the maximal derivative of the active nuclei density curve. Mean values were calculated for n embryos and error bars correspond to standard deviation.

https://doi.org/10.1371/journal.pgen.1007676.g002

MS2 reporter is reduced to less than 1% of posterior nuclei (Fig 2D). We confirm thus that Zelda maternal proteins contribute to the early expression of endogenous *hb* [32] and conclude that posterior expression of the *hb-MS2* reporter in early embryos is mostly due to Zelda.

The *MS2* cassette carries the cis-acting sequence responsible for *hb-MS2* posterior expression

To understand the discrepancies of expression between endogenous *hb* and the *hb-MS2* reporter at early cycles, we first aimed at identifying the minimal sequence sufficient to recapitulate early expression of the *hb* locus. While a transgene carrying 18 kb of the *hb* locus was shown to recapitulate *hb* anterior expression at nc13 and nc14, its expression at earlier cycles had not been documented [20, 21, 33]. RNA FISH, using a *hb* probe on embryos carrying a

single insertion of the *hb*-18kb BAC, reveals ongoing transcription at the three *hb*-encoded loci and indicates that expression of the *hb*-18kb BAC and endogenous *hb* largely overlap in the majority of anterior nuclei (Fig 3B). No RNA FISH signals are detected within the posterior domain of these embryos indicating that the *hb*-18kb BAC encompasses all the regulatory sequences to spatially control *hb* expression during early nuclear cycles.

Taking advantage of BAC recombineering, we generated *MS2-hb-18kb* transgenes carrying insertions of the MS2 cassette either in the 5'UTR within the intron of *hb* (*5'MS2-hb-18kb*) or in the 3'UTR of *hb* (*3'MS2-hb-18kb*). Expression of these new MS2 reporters was assessed by live imaging (S2 Movie) and double RNA FISH using a *hb* probe and an *MS2* probe. In the anterior of nc11 embryos either homozygous for the *5'MS2-hb-18kb* transgene (Fig 3C) or heterozygous for the *3'MS2-hb-18kb* transgene (Fig 3D), the *hb* probe reveals at most four spots of ongoing transcription : one at each of the two endogenous *hb* and two (C) or one (D) at the *MS2-hb-18kb* loci. In most cases, two of the *hb* spots co-localize with two (C) or one (D) *MS2* spot(s), which specifically label ongoing transcription at the *MS2-hb-18kb* loci. In these embryos, we also detect *hb* and *MS2* spots in posterior nuclei (Fig 3C and 3D), which co-localize for most of them, thus revealing ongoing transcription at the *MS2-hb-18kb* loci. Posterior expression of the *MS2-hb-18kb* loci is also detected in living embryos expressing the MCP-GFP (S2 Movie). Altogether, these data strongly argue that posterior expression of the *MS2-hb-18kb* transgenes is mediated by the MS2 cassette and suggest that Zelda-dependent posterior expression of the *hb-MS2* reporter is mediated by cis-acting sequences in the MS2 cassette.

The *hb* canonical promoter is sufficient to recapitulate early zygotic expression of *hb*

Given the trans-acting effect of Zelda on the posterior expression of the *hb-MS2* reporter (Fig 2) and the enhancer-like behavior of the MS2 cassette for posterior expression (Fig 3), we searched for potential Zelda binding sites in the MS2 sequence, using the ClusterDraw2 online algorithm [16] and Zelda position weight matrix [34]. The canonical Zelda binding site is a heptameric motif (CAGGTAG, Fig 4A) over represented in the enhancers of pre-cellular blastoderm genes [32, 35]. Strikingly, in the sequence of the MS2 cassette we find the motif CAGGTCG (a single mismatch with the canonical Zelda site) repeated 12 times and the motifs TAGGTAC (two mismatches) and TAGGCAA (three mismatches) each repeated 12 times (Fig 4B). This *in silico* analysis indicates that the MS2 sequence contained a total of 36 potential Zelda binding sites all located within linkers between MS2 loops (Fig 4B). Although we cannot be conclusive about the affinity strength of these various binding sites for Zelda, all of them share high similarity with TAGteam motifs [32]. We thus engineered a new MS2 cassette mutating the 36 putative Zelda binding sites of our original *hb-MS2* reporter and inserted this new MS2-ΔZelda cassette under the control of the *hb* canonical promoter as in the original *hb-MS2* reporter. Expression of this new *hb-MS2ΔZelda* reporter was assessed in living embryos expressing the MCP-GFP protein (S3 Movie). We do not detect any MS2 spots in the posterior of the embryo (Fig 5A) indicating that unlike our original *hb-MS2* reporter [26], the new *hb-MS2ΔZelda* reporter is expressed exclusively in the anterior at early cycles 10 to 11 as detected for endogenous *hunchback* by RNA FISH [3].

As RNA FISH are performed on fixed embryos whereas the MS2 data are obtained from live material, we wondered whether these two different approaches provide consistent quantification of *hb* transcriptional activity when focusing on the "steepness" of the expression boundary. Therefore, the probability to be active for *hb-MS2ΔZelda* loci at a given position along the AP axis and at a given time ($P_{SPOT}(t)$) was extracted from movie snapshots and compared to RNA FISH data of endogenous *hb* expression [3]. To compare data from several

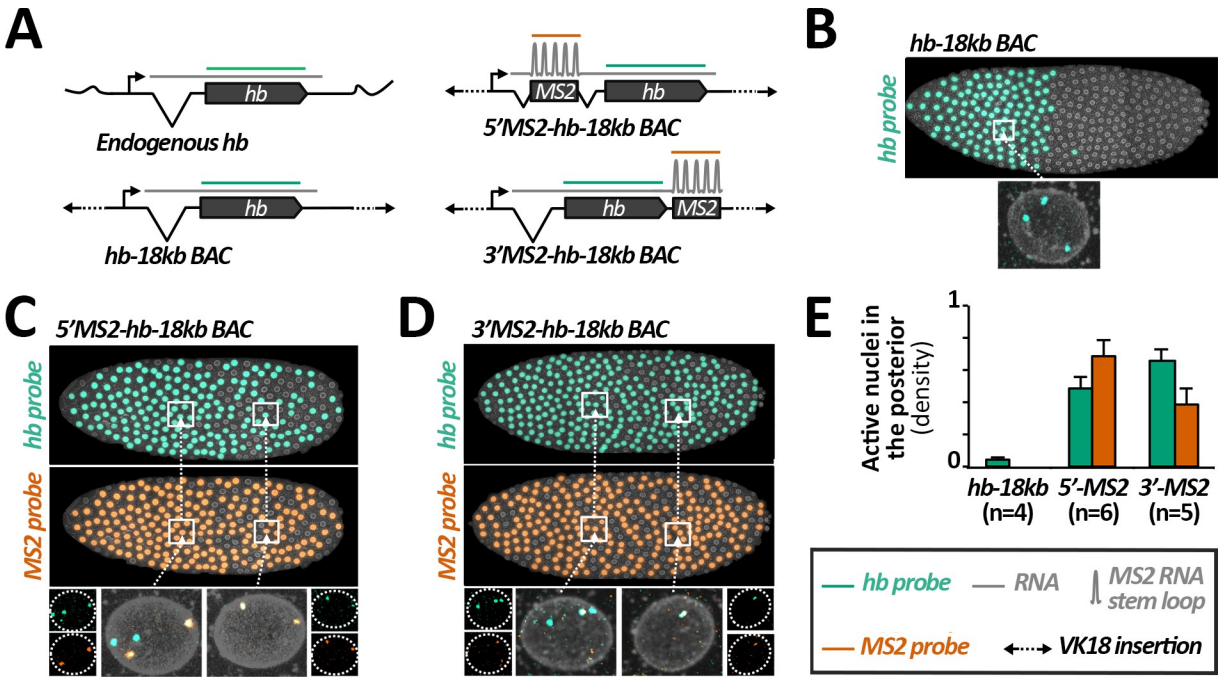

Fig 3. Posterior expression of the *hb-MS2* reporters is mediated *in cis* by the MS2 cassette. A) Structures of the *hb* expressing loci and relative positioning of the *hb* probe (green) or the *MS2* probe (orange) hybridizing to the transcripts. The *hb-18kb BAC* encompasses 18 kb of chromosome III spanning the *hb* locus. The 1.3kb MS2 cassette is inserted in the *hb-18kb BAC* within the intron of *hb*, 0.7kb downstream the transcription start site (*5'MS2-hb-18kb* BAC, top right) or within the 3'UTR of *hb*, ~ 3 kb downstream of the transcription start site (*3'MS2-hb-18kb* BAC, bottom right). All the BACs are inserted at the same position (VK18, chromosome II) within the fly genome. **B)** Top: Expression map of a typical nc11 embryo heterozygous for the *hb-18kb BAC* insertion. As highlighted on one example (bottom), nuclei in the anterior exhibit three sites of ongoing transcription detected with the *hb* probe: two of these sites correspond to expression at the endogenous *hb* loci and one of them corresponds to expression at the *hb-18kb* BAC locus. No expression is detected in the posterior. (**C-D)** Embryos are homozygous for the *5'MS2-hb-18kb* BAC insertion (C) or heterozygous for the *3'MS2-hb-18kb* BAC insertion (D). Top: Expression map of a typical nc11 embryo detected with the *hb* probe (green) and with the *MS2* probe (orange). Bottom: close-up of single nuclei in the anterior (left) and the posterior (right). **E)** Mean density of active nuclei in the posterior detected by the *hb* probe (green) or by the *MS2* probe (orange) on nc11 embryos carrying the *hb-18kb BAC* (*hb-18kb*), the *5'MS2-hb-18kb* BAC (*5'MS2*) or the *3'MS2-hb-18kb* BAC (*3'MS2*) insertion. Mean values are calculated for n embryos and error bars correspond to standard deviation.

https://doi.org/10.1371/journal.pgen.1007676.g003

embryos, embryos were aligned fixing the origin of the AP axis when the probability for a locus to experience transcription at any time during the interphase (P_{ON}) is equal to 0.5 (for the definition of the boundary see details in S3 Text). This embryo alignment allows us to

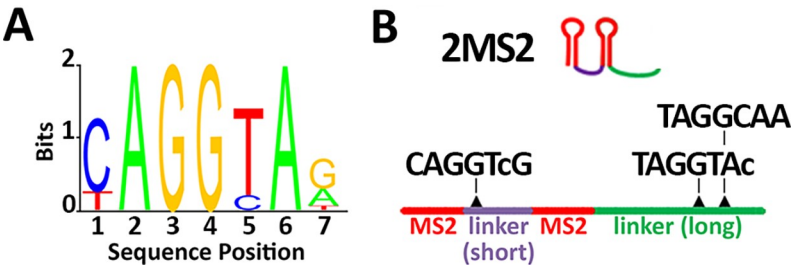

Fig 4. Zelda putative binding sites in the MS2 cassette. A) Position weight matrix of the Zelda binding site [34]. The critical positions in the canonical Zelda site C**AGG**TAG are highlighted in bold. **B)** The 24 MS2 stem loop repeat corresponds to 12 tandem repetitions of the two MS2 repeats shown. In this sequence, the MS2 loops (red) are separated by either a short (purple) or a long (green) linker. The short linker contains one CAGGTCG sequence which harbors a single but critical mismatch with the canonical Zelda site. The long linker contains one TAGGTAC and one TAGGCAA which harbor respectively two or three permissive (not critical) mismatches with the canonical Zelda site.

https://doi.org/10.1371/journal.pgen.1007676.g004

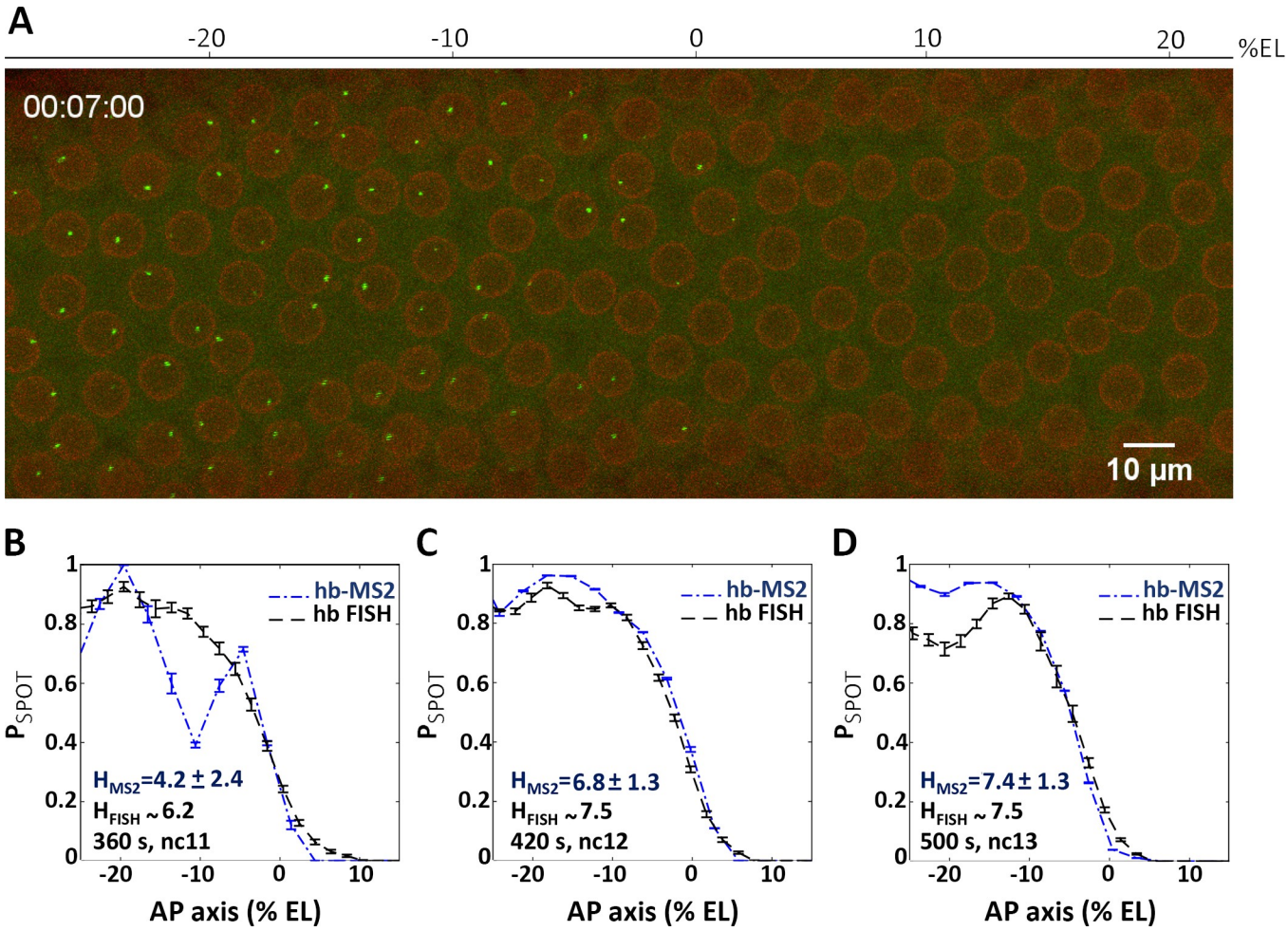

Fig 5. The *hb* canonical promoter expresses the *MS2ΔZelda* cassette in an anterior domain with a steep posterior boundary. (A) A 2D maximum projection snapshot from Movie3 (SI) was taken at ~7 minutes after the onset of nc12 interphase. In the green channel, MCP-GFP proteins recruited by the nascent MS2-containing mRNA can be seen accumulating at the *hb-MS2ΔZelda* loci (bright spots). In the red channel, the mRFP-Nup proteins localized at the nuclear envelope delineate nuclei. (B-D) Probability of active *hb-MS2ΔZelda* loci along the AP axis (dashed blue lines with error bars), extracted from snapshots of 6 movies near the end of each nuclear cycle: 360 s after the onset of nc11 interphase (B), 420 s after the onset of nc12 interphase (C) and 500 s after the onset of nc13 interphase (D). In each panel the probability of active endogenous *hb* loci (black dashed lines with error bars) extracted from the FISH data from [3] is also shown. Hill coefficients (H) are indicated in blue (*hb-MS2* reporter) or in black (endogenous *hb* from FISH data). In B, the difference between the FISH signal and the probability of active *hb-MS2ΔZelda* loci is due to small number of nuclei and large variability distance between them at nc11 which limit statistics.

https://doi.org/10.1371/journal.pgen.1007676.g005

compensate for input noise (variability in the Bicoid gradient), which was shown to be of about 2–3% EL [6], and focus only on the output noise (noise in the transcriptional response). Throughout the paper, we refer to average measures of expression by computing the probability of the locus to be ON as a function of position along the AP axis and as a function of time. We named this time-dependent probability to be ON, P_{SPOT} (t). P_{SPOT}(t) is thus a measure of the instantaneous gene activity at a given position along the AP axis and at a given time within the nuclear cycle. We first assigned a value of 1 to a nucleus that expresses the MS2-MCP gene above a certain threshold (see methods) at any time during the nuclear cycle. P_{SPOT}(t) is calculated by averaging over nuclei at a given position along the AP axis. We also use a cumulative P_{SPOT} named P_{ON}, which is used only for embryo alignment and which is a cumulative statistic per nuclear cycle. P_{ON} indicates the probability for a nucleus at a given position to experience transcription during nuclear cycle. A value of 1 is assigned to each nucleus experiencing transcription during the cycle

and P_{ON} is obtained by averaging over the nuclei at a given position. $P_{SPOT}(t)$ can decrease within a nuclear cycle if nuclei stop expressing, whereas P_{ON} cannot decrease.

As shown in Fig 5B–5D, the curves plotting the mean spot appearance $P_{SPOT}(t)$ as a function of position along the AP axis are similar when extracted either from the RNA FISH data (dashed line, [3]) or the MS2 movie snapshots (blue lines) with Hill coefficients varying from 4.5 (nc11) to ~ 7 at nc12 and nc13. Thus, the *hb-MS2ΔZelda* reporter is expressed at early cycles in an anterior domain with a boundary as steep as the boundary of the endogenous *hb* expression domain. These experiments show that the *hb* canonical promoter is sufficient to faithfully recapitulate the early zygotic expression of endogenous *hb*. This is in contradiction with our first interpretation [26] deduced from the expression of the original *hb-MS2* misleading reporter with its high number of unexpected Zelda binding sites. Nevertheless, the now almost perfect match between $P_{SPOT}(t)$ activity along the AP axis of the FISH data of endogenous *hb* expression and of the data extracted from movies of the *hb-MS2ΔZelda* reporter at the end of the interphase, ensures that the analysis of this reporter expression dynamics can help understand how the step-like expression of *hb* arises.

The *hb-MS2ΔZelda* reporter shows varying transcription kinetics in the anterior domain

The MS2 movies provide access to the transcription dynamics of each *hb-MS2 ΔZelda* single locus in all the visible nuclei of developing embryos. Key features are extracted from the time traces of the MS2-GFP spots (Fig 6A), choosing as the origin for time the onset of interphase for that particular nucleus (see details in S2 Text and S4 Fig). These features include: *i)* the initiation time (t_{init}) which measures the time period from the onset of interphase to the first detection of the MS2 transcription signal at the locus, *ii)* the time period during which the locus is activated (t_{active}) and *iii)* the time period at the end of interphase during which the locus is turned off (t_{end}). From the time traces (Fig 6A), the integral activity (ΣI) integrates the area under the trace and provides a relative measure of the total amount of mRNA produced. The average mRNA production rate (μI) is calculated by dividing ΣI by t_{active}. Features are obtained from 5 (nc11), 8 (nc12) and 4 (nc13) embryos. Embryos were aligned spatially fixing the origin of the axis at boundary position (P_{ON}) at nc12 and the origin of time was calculated for each nuclei as the origin of the respective cycle (see S2 Text and S4 Fig). As shown in Fig 6, several of these features exhibit different behaviors depending of the position along the AP axis. Notably, t_{init} and ΣI appear more variable when loci are located close to the boundary than in the most anterior part (Fig 6B–6G). Similarly, in a region of about 10% EL at the boundary, the mRNA production rate drops from the constant value reached in the anterior region to 0 at the boundary (Fig 6H–6J). Thus, the dynamics of the transcription process at the *hb-MS2ΔZelda* reporter exhibit two distinct behaviors: in the anterior of the embryo, time trace features are stable likely reflecting a maximum PolII loading rate and saturated levels of Bicoid; in a region of ~ 10% EL anterior to the expression boundary, time trace features are fluctuating reflecting limiting amounts of Bicoid. The pattern steepness corresponds to a Hill coefficient of ~7 to 8 of the regulation function (see S3 Text). The MS2 live imaging gives us the opportunity to really decipher the dynamics of the *hb* expression compared to the FISH that was just giving us $P_{SPOT}(t)$ for one arbitrary time point (probability for *hb* loci to be active at a given position along the AP axis and at the time of embryo fixation).

At each nuclear cycle, the *hb* expression pattern reaches steady-state in 3 minutes

The temporal dynamics of the *hb* pattern establishment at the scale of the whole embryo (along the AP axis) were extracted from the MS2 movies: the probability for the locus to be

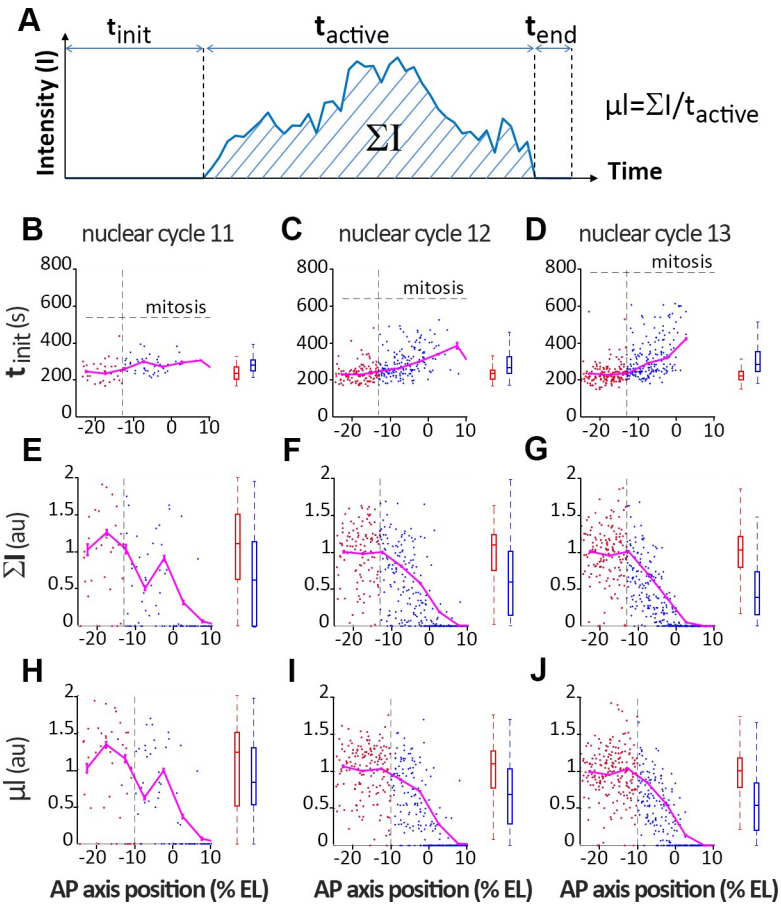

Fig 6. Distribution of time trace features along AP axis. (A) Description of the time trace features. Initiation time (t_{init}, B-D), normalized integral spot intensity (ΣI, E-G) and production rate (μI, H-J) are indicated as a function of position along the AP axis with the origin fixed for each embryo at the position of the expression boundary at nc12. Embryos were at nc11 (B, E and H), nc12 (C, F and I) and nc13 (D, G and J). The vertical dashed line indicates when the significant change in the feature distribution from the anterior pole is first detected in nc13, using the Kolmogorov-Smirnoff test (p-value 0.05). This line separates the *hb* expression domain into 2 zones: the anterior zone which exhibits a saturating process (red box) and the boundary zone which exhibit a more stochastic activity characterized by more variability (blue box). On the right of each panel (B-J), the distribution of the two populations is shown (median ± 25% and min/max). Example of MS2-MCP time traces are given in S1 Fig, S2 Fig and S3 Fig. Data were obtained from 5 (nc11), 8 (nc12) and 4 (nc13) embryos. All nc11 and nc12 traces were recorded for the whole duration of the cycle. Embryos were aligned spatially fixing the origin of the axis at the boundary position (P_{ON} = 0.5) at nc12 and the origin of time was calculated for each nuclei as the origin of the respective nuclear cycle (see S2 Text and S4 Fig). For t_{init}, the data points are for expressing nuclei only, whereas for ΣI and μI both expressing and non-expressing nuclei were taken into account.

https://doi.org/10.1371/journal.pgen.1007676.g006

ON as a function of the position along the AP axis and time in the cycle ($P_{SPOT}(t)$) can be visualized in S4 Movie and is plotted in the form of kymographs on pulled embryos as described above (Fig 7A–7C). At each cycle, spots can appear as early as ~ 150 s after mitosis. Given the interruption of transcription during mitosis, this limit of 150 s corresponds to the period required to re-establish transcription during the interphase and likely includes genome decondensation, the time it takes for the Bicoid protein to be imported in the nucleus after mitosis, and the time it takes for the MS2 system to produce a signal that is above background. After this period, expression rapidly turns on in the anterior to reach the plateau value where all nuclei express the reporter ($P_{SPOT}(t) \sim 1$). The time period to reach the plateau is shorter at the most anterior position in the field of view imposed by the movie recording (~ - 25% EL)

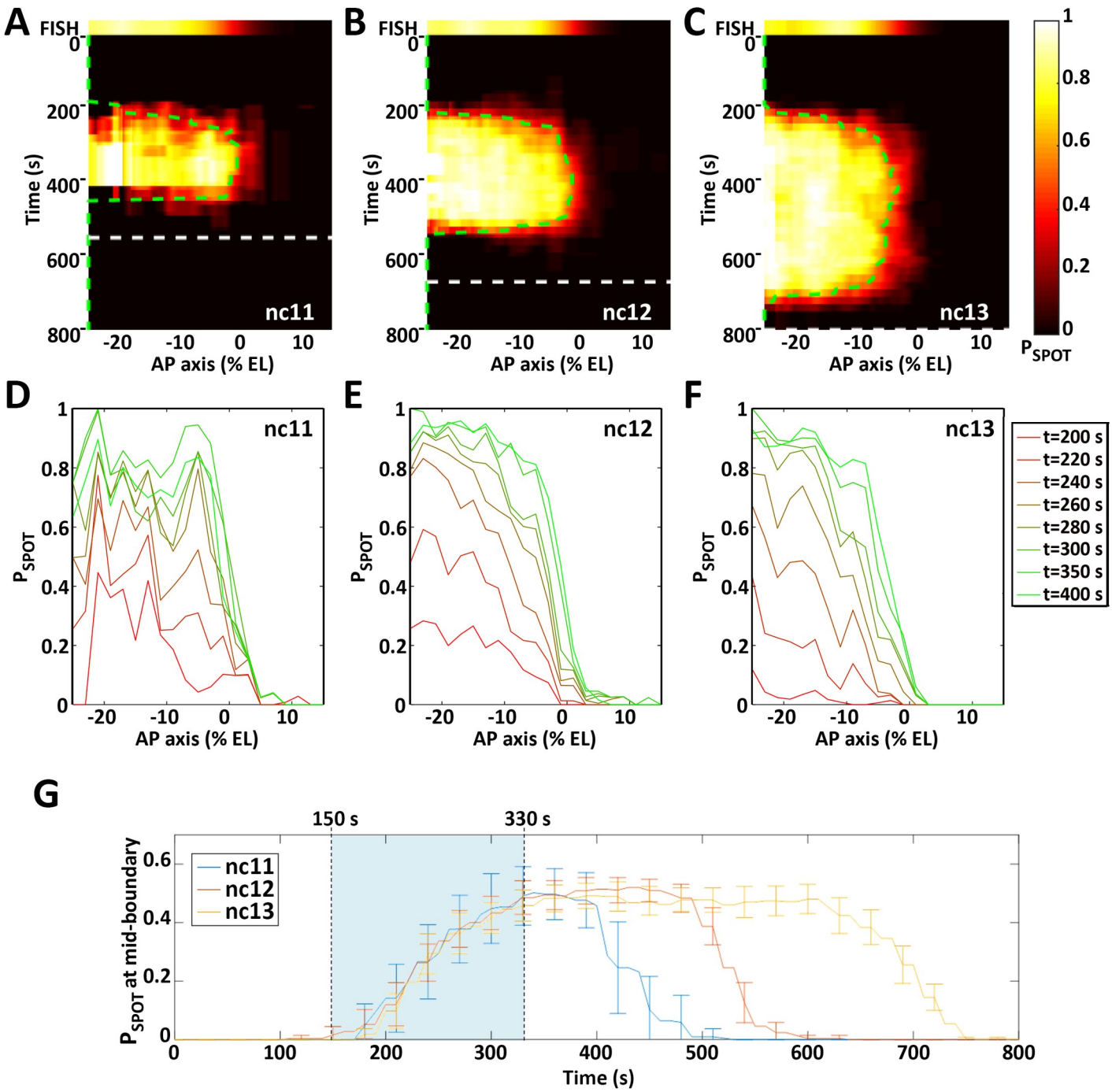

Fig 7. The dynamics of *hb-MS2ΔZelda* expression pattern. A-C: The probability for a given locus to be ON ($P_{SPOT}(t)$) is indicated by a heat map (color scale on the right where $P_{SPOT}(t) = 0$ is black and $P_{SPOT}(t) = 1$ is white) horizontally as a function of position along the AP axis (0% EL positioned where $P_{ON} = 0.5$ at nc12) and vertically as a function of time (s) fixing the origin at the onset of interphase for each nucleus (see details in S2 Text and S4 Fig). The top panel shows the endogenous *hb* expression pattern as measured from RNA FISH (15). For each cycle (**A**: nc11; **B**: nc12; **C**: nc13), the end of interphase (onset of the next mitosis) is indicated by a dashed line (white). The green dashed line indicates the position of the expression boundary ($P_{SPOT}(t) = 0.5$) over time. **D-F:** $P_{SPOT}(t)$ as a function of position along the AP axis for different times during the interphase of nc11 (**D**), nc12 (**E**) and nc13 (**F**). **G:** $P_{SPOT}(t)$ as a function of time (s) at the mid-boundary position (where $P_{SPOT}(t)$ reaches a steady value of 0.5). The first hints of transcription are observed at the mid-boundary position ~ 150 s after the onset of the interphase (lower limit of the light blue zone) and steady state is reached at ~ 330 s (higher limit of the light blue zone). The boundary formation reaches steady state in ~ 180 s. Data were obtained from 5 (nc11), 8 (nc12) and 4 (nc13) embryos. Embryos were aligned spatially by fixing the origin of the axis (0% EL) at the boundary position ($P_{ON} = 0.5$) at nc12 and the origin of time was calculated for each nuclei as the origin of the respective nuclear cycle (see S2 Text and S4 Fig).

https://doi.org/10.1371/journal.pgen.1007676.g007

and increases with the distance to the anterior pole (Fig 7D–7F) consistent with a dose-dependent activation process of *hb* by Bicoid [4, 8]. Then, the expression pattern is steadily established, which includes fixing the boundary position and steepness (see S4 Text for measurement details). This stable state lasts for a period of time which varies with the length of the cycle until *hb* expression rapidly gets switched off simultaneously at all positions along the AP axis: at 400 s at nc11 (Fig 7A & 7G), 500 s at nc12 (Fig 7B & 7G) and 750 s at nc13 (Fig 7C & 7G). Importantly, the dynamics of the boundary positioning is the same at the three nuclear cycles considered (Fig 7G) and the steady state of boundary positioning is reached rapidly: ~330 s after the onset of the cycle corresponding to ~ 180 s after the first hints of transcription at this position (Fig 7G). Dynamics of pattern steepness and average spot intensity also exhibit similar behaviors (see S5 Text and S9 Fig, respectively). Thus, expression of the *hb-MS2ΔZelda* reporter allows us to directly observe position-dependent transcriptional activation, which is consistent with Bicoid dose-dependent transcriptional activation. Also, it demonstrates that the steady-state of positional measurement is reached in no more than 3 min at each cycle with very similar dynamics between cycles. Once the steady state is reached, the *hb* boundary is fixed around the position ~ -5% EL.

Modeling the Bicoid-mediated dynamics of the *hb* expression pattern

To better understand how the stable response downstream of Bicoid is achieved, we build a stochastic model of *hb* expression regulation by the Bicoid transcription factor (TF), coupled with a stochastic transcription initiation process assuming random arrival of RNA polymerases when the gene is activated. The mechanism of *hb* expression regulation through the cooperative binding of multiple TFs to the promoter was originally proposed in 1989 to explain how the shallow Bicoid gradient could give rise to an expression pattern with a steep boundary [8, 9]. It was subsequently proposed [36] that within an equilibrium binding model, a pattern steepness quantified by a Hill coefficient of N requires a promoter with at least N TF binding sites. Here, we consider a model with N TF binding sites, where the promoter state P_i is decribed by the probability of having i TF bound at a given time (Fig 8A). Transitions between the states occur via binding and unbinding events of TF to the sites. We assume an equilibrium binding model, in which all transitions are reversible and the binding sites are identical. As a result the state of the promoter is described solely by the number of bound TF, and not their position on the *cis* regulatory array. We assume that gene expression is activated only when all N binding sites are bound by TF. In the regime of parameters corresponding to a high pattern steepness, this "all-or-nothing" assumption is shown to have very limited impact on the pattern dynamics (see [29] and our companion paper, [37]). Following this activation, RNA polymerases can arrive to the promoter in a Poisson process and initiate the downstream transcription initiation process. Our simplified model does not account for a non constant polymerase arrival rate [38].

We investigate the *hb* pattern dynamics by solving a stochastic time dependent master equation (Eq 7 in S6 Text) and considering binding rates that vary as a function of TF concentration *[TF]*: at the boundary position, TF concentrations are lower than in the anterior region [5, 39] and it takes more time for a diffusing TF to reach binding sites at the promoter than in the anterior region where TF concentration is higher. The value of the binding rate constants is further limited by the value of the diffusion coefficient (see S6 Text, 1). In our model, the cooperativity between the binding of TFs is modeled implicitly by the value of the unbinding rates of the TF to the binding sites: higher cooperativity corresponds to higher stability of the promoter state with N bound TF, which is modeled through a lower unbinding rate. The unbinding rate is limited at the boundary so that P_{SPOT} (t) = 1/2. Meanwhile, the unbinding

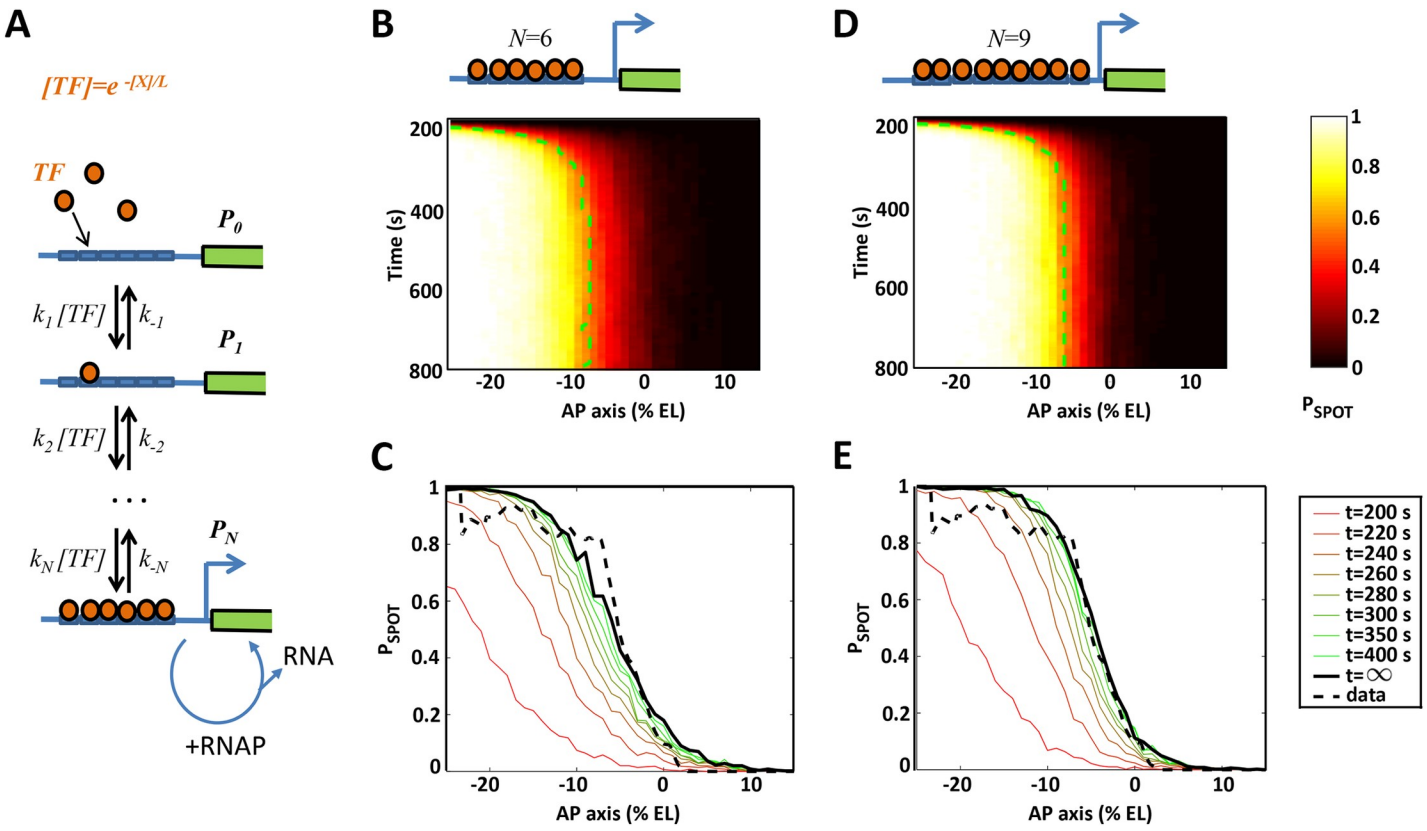

Fig 8. Modeling transcriptional regulation by the Bicoid transcription factor through interactions with the *hb* promoter operator sites. A) A model of regulation by Bicoid transcription factor (TF) binding to multiple binding sites on the *hb* promoter coupled with stochastic transcription initiation. Transcription initiation is allowed only when the binding sites are fully bound. During this window, RNAP can randomly bind to the promoter and initiate transcription to produce mRNA. **B or D**) The model prediction for the probability of an active transcription locus ($P_{SPOT}(t)$, colorbar) as a function of time in the nuclear cycle and position along the AP axis for a model with 6 (**B**) or 9 (**D**) Bicoid binding sites. **C or E**) The simulated pattern evolution of $P_{SPOT}(t)$ along the AP axis over time (colored line), shown with the pattern predicted at steady state (solid black line) and the stable pattern extracted from the data in nc13 (dashed black line, as in Fig 7F). Panels **C** and **E** represent cuts in time of panels **B** and **D**, respectively. The kinetic parameters were chosen so as to match the observed *hb* pattern steepness and formation time at the boundary ($P_{SPOT}(t) = 0.5$) (see S2 Table). The value of $P_{SPOT}(t)$ is calculated from 200 trajectories per AP position.

https://doi.org/10.1371/journal.pgen.1007676.g008

rate constants are kept constant along the AP axis (independant of Bicoid concentration) but differ depending on the occupancy state of the promoter to account for copperativity. At time t = 0, all binding sites are free of TF.

Motivated by the 6 known Bcd binding sites on the *hb* promoter [8, 17], we first consider a model with 6 binding sites ($N = 6$). The binding and unbinding rates are chosen (Eq 5 in S6 Text) to achieve the closest steepness and establishment period to the *hb* pattern observed in the movies (Fig 7A–7C). The model fits are performed on data pulled from all embryos and nuclear cycles. The gene expression pattern dynamics, shown as the probability ($P_{SPOT}(t)$) of a nucleus having an active locus (bright spot) as a function of position along the AP axis and as a function of time during the nuclear cycle, shows a good qualitative agreement between the model and the data. In Fig 8B, similarly to Fig 7A–7C, initially there is no expression since the TF are not bound to the promoter. Active transcription loci first appear near the anterior pole, where the activator concentration is the highest, and then transcription activation propagates quickly to the mid-anterior region. After a certain amount of time, the steep expression pattern becomes stable, with the boundary (dashed green line) located near the mid-embryo region where the *hb* boundary is located. However, using the canonical number of binding sites

($N = 6$) results in a steepness of the boundary lower than that observed in the experimental data (Fig 8C). Increasing the binding sites number from 6 to 7, 8, 9 or 10 allows us to match the observed boundary steepness to the experimental data (H~7). Yet, we have shown in a companion manuscript [37] that the steeper the patterns are, the longer the time needed for them to establish. Specifically, obtaining the observed Hill coefficient of H~7 in 3 minutes is not possible with 7 or 8 binding sites but requires 9 binding sites (Fig 8E). Increasing N beyond 9 did not result in a significantly better fit (see S6 Text, 5).

Discussion

In this study we show that the removal of 36 putative binding sites for the transcription factor Zelda (unfortunately present in the sequence of the MS2 cassette) reveals a new temporal dynamics of the *hb* canonical promoter at the onset of zygotic transcription. Unlike our original *hb-MS2* reporter [26], the new *hb-MS2ΔZelda* reporter faithfully reproduces the early zygotic expression of the endogenous *hb* observed with RNA FISH [3, 26]. It indicates that the 750 bp of the *hb* locus, including 300 bp of the proximal enhancer, the P2 promoter and the intron, are sufficient to reproduce the endogenous expression of the *hb* gene in the early nuclear cycles (11 to 13). The dynamics of establishment of the *hb* pattern at these early stages of development is thus properly captured by the new *hb-MS2ΔZelda* reporter.

These MS2 movies provide access to the *hb* pattern dynamics, which was not perceivable in previous *in situ* experiments on fixed embryos. *hb* expression first occurs in the anterior then proceeds to the boundary region. A difference in the activation time (initiation time) following mitosis is observed even within the anterior region, allowing us to visualize for the first time position-dependent activation of *hb* and thus likely dose-dependent activation by Bicoid. Analysis of the MS2 time traces indicates that the transcription process is more variable among nuclei at the boundary of the expression domain, where Bicoid concentration is low and probably limiting, than in the anterior where the concentration of Bicoid is high. Tailor-made analysis of the time traces allowed us to extract different kinetic parameters of promoter activity in these two regions and to demonstrate that transcription of the *hb-MS2ΔZelda* reporter is bursty (described by a two state model) in both regions [40]. This anti-correlation between the relative variability of mRNA production among nuclei and the Bicoid concentration (position along the AP axis) supports the idea that Bicoid interactions with the *hb* promoter are rate-limiting processes contributing to "bursty" transcription. Nevertheless, rate-limiting interaction of Bicoid with DNA is not the sole factor contributing to bursty transcription, as it is also observed in the anterior region with very high Bicoid concentration [40]. Thus, despite extremely fast transcription initiation imposed by the 5 min interphase and frequent mitoses, bursty transcription is clearly observed at the onset of zygotic transcription in fly embryos.

The MS2 movies indicate that the *hb* boundary is established within 3 minutes at each nuclear cycle with a very high steepness (H ~7). How the steepness and positioning of the boundary are reached so rapidly is unclear. Our data (Fig 6 and Fig 7) indicate that it takes more time for *hb* expression to reach steady-state levels in the boundary region and that Bicoid is thus likely to be a rate-limiting factor in the formation of the *hb* pattern around the boundary region. The time scale of interactions (i.e. binding and unbinding) of Bicoid with the *hb* promoter is critical in determining how quickly the accurate *hb* response is established. Therefore, the interactions between Bicoid molecules and the *hb* promoter need to be modeled explicitly, rather than implicitly. We propose an equilibrium model of transcription regulation via the binding/unbinding of transcription factors to the operator sites of the target promoter.

This model can account for various types and degrees of cooperativity between the binding of TFs, from which a steep *hb* pattern can emerge [29].

Using this model, we show in a tandem paper that accommodating a steep gene expression pattern within the considered model requires very slow promoter dynamics and thus would result in a very long pattern formation time [37]. Considering this trade-off, the steepness and the pattern formation time observed from the movies are even more intriguing. The most relevant model with 6 binding sites, motivated by previous work [8], fits well the pattern dynamics but fails to reproduce the observed steepness of the boundary in such a short time period of 3 min. The failure of the 6 binding sites model to completely reproduce the experimental data indicates that the assumption that 6 binding sites for Bicoid are sufficient for the observed response is wrong and that additional mechanisms have to be included in the model to enhance the steepness of the boundary to the observed level. It was recently proposed that energy expenditure, encoded as non-equilibrium binding of the TF, can allow a Hill coefficient greater than the number of binding sites (up to 11 with 6 sites) [29]. Alternatively, different regulatory scenarios could play a role. First, we found that increasing the number of binding sites up to 9 allows a significantly better fit of the model with the data than with 6 binding sites. It is thus possible that the 750 bp of the *hb* gene that are sufficient to elicit the pattern contain more than 6 Bicoid binding sites. As recently pointed out, the importance of low affinity binding sites might be critical to confer specificity and robustness in expression [37] and a closer analysis of the *hb* regulatory sequence looking for potential weak binding sites for Bicoid might clarify this point. A second possibility is the involvement of other transcription factors distributed as gradients that could bind to the *hb* promoter and contribute to the increase in the steepness of the boundary. The Hb maternal protein, which is also expressed as an anterior to posterior gradient and able to bind to the endogenous *hb* promoter [38], contributes to the *hb* expression process by allowing expression at lower Bicoid concentration thresholds [12] and faster activation [15]. Although this has not yet been investigated, maternal Hb might also contribute to sharpen the *hb* boundary in a timely manner. Alternatively, maternal repressors expressed as gradients in the posterior region or downstream of the boundary could also contribute to the steepness of the *hb* boundary. Among potential candidates are Caudal, which is expressed as a posterior to anterior gradient but so far has been described as a transcriptional activator in fly embryos [41], or Capicua, a transcriptional repressor at work in the center of the AP axis, where the *hb* boundary forms [7].

From the movies, the dynamics of establishment (before reaching steady state) of the *hb* pattern appears to be invariant at the three nuclear cycles considered (nc11, nc12 and nc13). At these three nuclear cycles, it takes ~180 s from the detection of the first MS2-MCP spots to the establishment of the pattern near the mid-embryo position (Fig 7G). This invariance in the dynamics of establishment indicates that there are no dramatic changes in the regulation of the transcription process during the three cycles suggesting that Bicoid remains one of the main patterning factors of *hb* transcription dynamics at the boundary region in these stages of development. The other transcription factors involved in *hb* expression [15, 19], if any, would need to be stably maintained during the three cycles. As mentioned above, one possible factor is the Hb protein itself, which was shown to contribute to the expression of the *hb* expression pattern with both a maternal and a zygotic contribution [12, 15]. A likely hypothesis is that up to nc13, the zygotic Hb protein production is balanced by maternal Hb protein degradation, thus leading to a stabilized Hb gradient over the three considered cycles.

Previous observations of Bicoid diffusion in the nucleus space pointed out that it requires at least 25 minutes for a single Bicoid binding site to sense the Bicoid concentration with 10% accuracy, a level observed using FISH and protein staining experiments [5, 15, 39]. This estimation is based on the Berg-Purcell limit in the precision of concentration sensing of diffusing

molecules via surface receptors [42–44]. It should be noted that the Berg-Purcell limit applies when the interactions between the binding sites and the TF are independent. This limit for the Bicoid/*hb* system results in a non-steep gene expression pattern ($H \sim 1.31$, see S2 Table). In-depth analysis of the model in the tandem paper [45] shows that increasing the pattern steepness slows down the switching rate between the gene's active and inactive states, due to the required cooperativity between the binding sites [29]. Consequently, our fitted models (with $N = 6$ or $N = 9$ binding sites) result in much higher errors in the integrated readout when compared to the model of independent binding sites (S12 Fig), and require a significantly longer integration time to achieve a specific precision level. Thus, the answer to the precision of the *hb* pattern achieved in such a short interphase duration remains elusive. In the future, systematic studies using synthetic promoters with a varying number of Bicoid binding sites and quantitative analyses of promoter dynamics captured with the MS2-MCP system will help characterize not only the cooperativity of Bicoid binding sites but also the kinetics of the downstream processes once the gene is activated. Added to this, the Bicoid search time for its binding sites on *hb* [15, 39] also needs to be revisited. The employed value (~4 s) in our model is estimated assuming a 3D search process inside the nucleus space but if Bicoid can slide along DNA in search for the sites, the process can be ~100 times faster [46]. Such a possibility is compatible with fluorescence correlation spectroscopy measurements of Bcd-eGFP motion [15, 47] and the recent observed clustering of the Bicoid molecules across the embryo [48]. The advent of single molecule tracking methods [48, 49] represent a promising approach to further shed lights on the mechanism of this process.

Importantly, despite these very rapid and precise measurements of Bicoid concentration along the AP axis, the expression process itself shows great variability in the total amount of mRNA produced during the interphase per nucleus ($\delta mRNA/\langle mRNA \rangle$ ~150% in the boundary region) [40]. It is thus difficult to gauge to which degree errors in sensing Bicoid concentration contribute to the variability of the total mRNA produced at the boundary [40]. This also raises the question of understanding how precision in the downstream processes required for embryo segmentation is achieved at the scale of the whole embryo. If the embryo is capable of spatially averaging *hb* expression between nuclei at the same AP position (for example by the diffusion and nuclear export of its mRNA and nuclear import of its protein) [25], this will help the system distinguishing between the anterior and posterior region based on the *hb* transcription pattern alone. However, spatial averaging has a limit, due to the very short time available, the limited number of nuclei and the finite diffusion coefficient of the *hb* gene products [25]. It is likely that nuclei need to integrate *hb* gene expression over the nuclear cycle to reduce the noise in the *hb* readout. In nc11, the pattern collapses soon after reaching steady-state due to the next mitosis round. Therefore, any integrations of gene expression in nc11 and earlier (interphase duration shorter than ~400 s) are likely to lead to bias the pattern boundary to the anterior. Only starting at nc12 is the interphase duration long enough to reliably produce a steep pattern with the border around the mid-boundary position, based on the number of mRNA produced per nucleus (ΣI).

Materials and methods

Drosophila stocks

The original reporter *hb-MS2* and the Nup-RFP and MCP-GFP transgenes, both inserted on the second chromosome, were from [26]. All transgenic stocks generated in this study were obtained by BestGene. The $zld^{294}FRT19A$ chromosome was a gift from C. Rushlow [32] and female germline clones were induced using heat-shock FLP recombinaison [50] with a *OvoD1hsFLPFRT19A* chromosome (# 23880, Bloomington). All stocks were raised at 25˚C.

Plasmids and BACs

The *hb-18kb-BAC* spanning the *hb* locus was the BAC CH322 55J23 obtained from PACMAN BAC libraries [51]. The *24xMS2 cassette* was inserted in the 5'UTR within the *hb* intron (*5'MS2-18kb-BAC*) or in the 3'UTR (*3'MS2-18kb-BAC*) using BAC recombineering [52] (details in S1 Text). The plasmid used to generate the new *hb-MS2ΔZelda* reporter was generated by replacing in the *pCasPeR4-hb-MS2* construct from [26], the MS2 cassette by a new MS2 sequence synthetically generated by Genscript in which all putative Zelda binding sites (*24xMS2-SL-ΔZelda*) had been mutated. The sequence coding for the CFP in the *pCasPeR4-hb-MS2* construct from [26] was also replaced by the sequence coding the iRFP (Addgene 45457) in which a unique putative Zelda binding site had been mutated (See S1 Text for more information).

The MS2-SL-ΔZelda sequence

Sequence-based binding-site cluster analysis was performed using the online software ClusterDraw2 v2.55 at line.bioinfolab.net/webgate/submit.cgi. PWM for Zelda has been generated from [34] using the following Zelda binding sites: CAGGTAG; CAGGTAA; TAGGTAG; CAGGTAC; CAGGTAT; TAGGTAA; CAGGCAG and CAGGCAA. All heptamers detected as being a potential Zelda binding sites have been mutated and the new sequence synthesized by Genscript. The sequence of the new MS2 ΔZelda cassette is given in S1 Text.

RNA FISH and analysis

Embryo fixation and RNA *in-situ* hybridization were performed as describe in [3]. Briefly, RNA probes were generated using T7/T3 *in-vitro* transcription kit (Roche). *hb* RNAs were labelled with digoxigenin-tagged anti-sense probes detected with a sheep anti-dig primary antibody (1/1000 dilution, Roche) and donkey anti-sheep Alexa 568 secondary antibody (1/400 dilution, Invitrogen). MS2 containing RNAs were labelled with biotin-tagged anti-sense probes detected with a mouse anti-bio primary antibody (1/400 dilution, Roche) and chicken anti-mouse Alexa 488 secondary antibody (1/400 dilution, Invitrogen). Embryos were incubated 10 min with DAPI for DNA staining and 10 min in WGA-Alexa 633 (1/500 dilution, Molecular Probes) for nuclear envelop staining. Fixed embryos were mounted in VectaShield (Vector) and imaged in 3D (~20Z x 0.45μm) with a XY resolution of 3040*3040, 8bits per pixels, 0.09μm pixel size, 1 airy unit using a Zeiss LSM780 confocal microscope with a Zeiss 40x (1.4 NA) A-Plan objective. A full embryo 3D RAW image is composed on three 3D RAW Images that were stitched using Stitch Image Grid plugins from FIJI with 10% overlap and the linear blending fusion method. Image processing and analyzing were performed as describe [26]. Embryos of the proper stage in the nc11 interphase were selected according a threshold based on the nuclear area above 80 μm^2 (corresponding to late interphase) as in [3]. The expression map of endogenous *hb* or *MS2* transgenes have been manually false colored on FIJI and flatten on the nuclear channel.

Live embryo imaging

Imaging conditions were comparable to those outlined in [26, 53]. Embryos were collected 1h after egg laying, dechorionated by hand, fixed on the cover slip using heptane-dissolved glue, and immersed in to halocarbon oil (VWR). Mounted embryos were imaged at ~ 25˚C on a Zeiss LSM780 confocal microscope with a Zeiss 40x (1.4 NA) A-Plan objective. Image stacks of the lower cortical region of the embryo close to the middle of the AP axis (pixel size 0.2 μm, 0.54 μs pixel dwell time, 8 bits per pixels, confocal pinhole diameter 92 μm, distance between consecutive images in the stack 0.5 μm, ~1200x355 pxl, ~30 z-stacks) were collected

continuously. The GFP and RFP proteins were excited with a small fraction of the power output of a 488nm and a 568nm laser, 1.2% and 2% respectively. Images were acquired using the ZEN software (Zeiss). For each embryo, a tiled image of the midsection of the whole embryo was obtained, by stitching 3 separate images, from which the position of the anterior and posterior poles could be inferred.

Image processing and data extraction

Live imaging processing was performed in MATLAB as in [26]. Following imaging, movies are checked manually to verify all the nuclei included in data analysis are fully imaged in their depth and incompletely imaged nuclei (mostly nuclei at the periphery of the imaging field) are excluded. Nuclei segmentation is performed in a semi-automatic manner using our own software [54]. Only nuclei that exist throughout the nuclear interphase are used for the analysis. The MS2 spot detection was performed in 3D using a thresholding method. An average filter was applied before thresholding on each Z of the processed time point for noise reduction. MS2 spots were detected by applying a threshold equal to ~2 fold above background signal and only the spots composed of at least 10 connected voxels were retained. The intensity of the 3D spot is calculated as the sum of the voxel values of each Z-stack. At the end of nc13, some MCP aggregates may cause false spot detections: they are less bright and their shape is more spread compare to the MS2-MCP spots. The aggregates are eliminated automatically by raising the spot detection threshold without affecting the detection of the MS2 spots. We manually checked each movie to ensure the correct spot detection. The data from a segmented movie indicates for each nucleus its segmentation profile, identifier number and the intensity trace of the detected spot over time.

During mitosis, nuclei divide in waves, usually from the embryo poles. Therefore, nuclei at the anterior pole may produce MCP-MS2 spots earlier due to either earlier chromatin decondensation or earlier reentrance of Bicoid into the nucleic space [6]. We correct for this by realigning all the intensity traces by choosing the origin for time for each trace when the two sibling nuclei are first separated (see S2 Text and S4 Fig)

Stochastic model of *hb* expression regulation

The general model of transcription regulation through transcription factor (TF) binding/unbinding to the operator sites (OS) is a based on a graph-based linear framework [29, 55, 56]. We introduce a single time scale, which is the TF search time for a single operator site at the boundary t_{bind} ~ 4s. The details of the model are described in S6 Text and S7 Text.

Supporting information

S1 Text. Supplementary molecular biology.
(PDF)

S2 Text. Determining the origin of time for each time trace.
(PDF)

S3 Text. Embryo alignment.
(PDF)

S4 Text. Quantifying the steepness of *hb* expression pattern.
(PDF)

S5 Text. Evolution of the transcription pattern steepness over time.
(PDF)

S6 Text. Models of transcription factor (TF) sensing and transcription.
(PDF)

S7 Text. Comparing the noise in positional readout between models.
(PDF)

S8 Text. Supporting References.
(PDF)

S1 Fig. Examples of individual spot intensity over time in nuclear cycle 11. The time traces are sorted by their respective nuclei position, which is shown in the boxes in % EL (Position 0 corresponding to the middle of the embryo). Nuclei with position beyond -3.1% EL (last shown nucleus) have no spots. Horizontal axis: time in seconds. Vertical axis: spot fluorescent intensity in arbitrary units.
(PDF)

S2 Fig. Examples of individual spot intensity over time in nuclear cycle 12. The time traces are sorted by their respective nuclei position, which is shown in the boxes in % EL (Position 0 corresponding to the middle of the embryo). Nuclei with position beyond 6.6% EL (last shown nucleus) have no spots. Horizontal axis: time in seconds. Vertical axis: spot fluorescent intensity in arbitrary units.
(PDF)

S3 Fig. Examples of individual spot intensity over time in nuclear cycle 13. The time traces are sorted by their respective nuclei position, which is shown in the boxes in % EL (Position 0 corresponding to the middle of the embryo). Nuclei with position beyond -1.5% EL (last shown nucleus) have no spots. Horizontal axis: time in seconds. Vertical axis: spot fluorescent intensity in arbitrary units.
(PDF)

S4 Fig. Determining the nuclei birth time. (A) Examples of frame-by-frame monitoring of two sibling nuclei after mitosis. The time interval between frames is 13.05 s. The yellow line is drawn automatically to connect the two siblings' centroids once division is detected. (B) The distance between the centroids (blue line) and its derivative (red line) over time. The nuclei's birth is set as the time when the speed of segregation between the sibling nuclei decreases to near-zero. (C) Examples of the nuclei birth time t_{birth} along AP axis. Shown is the t_{birth} extracted from the movies (blue circles) and from the fitted model in Eq 1 (red dashed line). The y axis (t_{birth}) is shifted so as the two mitotic waves from the two poles meet at $t_{meet} = 0$.
(PDF)

S5 Fig. Fitting the trace feature patterns in nuclear cycle 11. The fitted curves (dashed black lines) are shown with data points (blue dots). Each data point corresponds to a single trace feature value. The horizontal axis is the AP axis in % EL.
(PDF)

S6 Fig. Fitting the trace feature patterns in nuclear cycle 12. The fitted curves (dashed black lines) are shown with data points (blue dots). Each data point corresponds to a single trace feature value. The horizontal axis is the AP axis in % EL.
(PDF)

S7 Fig. Fitting the trace feature patterns in nuclear cycle 13. The fitted curves (dashed black lines) are shown with data points (blue dots). Each data point corresponds to a single trace's

feature value. The horizontal axis is the AP axis in % EL.
(PDF)

S8 Fig. Time evolution of the pattern steepness H(t) over time. Shown for nc 11 (blue solid line), nc 12 (red solid line) and nc 13 (yellow solid line) along with the margins of errors (p-value = 0.05). Also shown (dashed lines) are the Hill coefficients extracted from FISH data in for the respective cycles. The coefficients from FISH in nc12 and nc13 are almost identical.
(PDF)

S9 Fig. Dynamics of *hb-MS2ΔZelda* expression (mean spot intensity) as a function of time. **A-C**: The average spot intensity I(t) is indicated by a heat map (color scale on the right) horizontally as a function of position along the AP axis (0% EL positioned P_{ON} boundary at nc12) and vertically as a function of time (s) fixing the origin at the onset of interphase for each nucleus (see details in S2 text and S4 Fig). For each cycle (**A**: nc11; **B**: nc12; **C**: nc13), the end of interphase (onset of next mitosis) is indicated by a dashed line (white). The green dashed line indicates the position of the expression boundary (I(t) equals half the average spot intensity at the anterior pole) over time. **D:** I(t) as a function of time (s) at mid-boundary position. The first hints of transcription are observed at mid-boundary position ~ 170 s after the onset of interphase (lower limit of the light blue zone) and steady state is reached at ~ 350 s. Boundary formation reaches steady state in ~ 180 s. Data were obtained from 5 (nc11), 8 (nc12) and 4 (nc13) embryos. Embryos were aligned spatially fixing the origin of the axis at boundary position (P_{ON}) at nc12 and the origin of time was calculated for each nuclei as the origin of its respective cycle (see S2 Text and S4 Fig).
(PDF)

S10 Fig. MS2 binding site configuration. *L(t) is* the number of MS2-MCP binding sites on a nascent RNA at time *t* after its transcription initiation.
(PDF)

S11 Fig. Examples of simulated trajectories at mid-embryo for $N = 6$. (A) The number of bound TF molecules to the promoter over time. (B) The gene transcriptional state given the number of bound molecules to the promoter. The gene is turned ON when the promoter is fully bound by TF. (C) Occurrences of transcription initiation events $I_{RNAP}(t)$, corresponding to (B). (D) Transcription loci intensity $I(t)$, corresponding to (C).
(PDF)

S12 Fig. Comparing the relative noise in the positional readout $\delta mRNA/\langle mRNA \rangle$ as a function time. For fitted model with $N = 6$ (blue line), fitted model with $N = 9$ (red line) and "no cooperativity" model (yellow line).
(PDF)

S1 Table. Parameters of fitting the sigmoid function with time trace features in nc11-13. The position of the feature pattern border (X_0, in units of % EL), the pattern steepness (H) and their respective confidence interval (in brackets) for the locus activity (P_{active}), the time period during which the locus is activated (t_{active}), the integral transcription activity (ΣI) and the mean transcription rate (μI). The data are inferred from all aligned embryos in the respective cycles.
(PDF)

S2 Table. Fitted models of varying number of operator sites *N* and the model of 6 independent sites. Shown is the p-value of the likelihood ratio test between the fitted model of *N* and *N-1* OS. Also shown is the Bayesian Information Criterion (BIC) for each model. The data for

the fitting is pulled from all embryos in all nuclear cycles.
(PDF)

S1 Movie. Live imaging of transcription dynamics of *hb-MS2 (Lucas et al. 2013)* subject to varying doses of Zelda. (A) Zelda hetero (Zld Mat +/-): expression of the *hb-MS2* reporter in embryos from zld^{294} heterozygous females. (B) Zelda GLC (Zld Mat -/-): expression of the *hb-MS2* reporter in zld^{294} germline clone embryos. The movies have two channels: MCP-GFP channel (green) for monitoring the dynamics of nascent mRNA production and NUP-RFP (red) for nuclei detection. The capture frame is from -25% to 25% of embryo length. The anterior pole is on the left side of the frame.
(AVI)

S2 Movie. Live imaging of the transcription dynamics with the MS2 cassette inserted at 5'-UTR and 3'-UTR. The MS2 cassette *(Lucas et al. 2013)* is placed at the (A) 5'-UTR within the intron of the *hb* gene (*5'MS2-hb-18kb*) and the (B) 3'-UTR of *hb* gene (*3'MS2-hb-18kb*). The movies have two channels: MCP-GFP channel (green) for monitoring the dynamics of nascent mRNA production and NUP-RFP (red) for nuclei detection. The capture frame is from -25% to 25% of embryo length. The anterior pole is on the left side of the frame.
(AVI)

S3 Movie. Live imaging of transcription dynamics of *hb-MS2ΔZelda*. Expression of the *hb-MS2ΔZelda* reporter in wild-type embryos. The movie has two channels: MCP-GFP channel (green) for the monitoring of nascent mRNA production dynamics and NUP-RFP (red) for nuclei detection. The capture frame is from -25% to 25% of embryo length. The anterior pole is on the left side of the frame.
(AVI)

S4 Movie. The transcription pattern dynamics in nuclear cycle 13. The movie shows the transcription patterns, represented by the probability of spot appearance $P_{SPOT}(t)$ along AP axis, at a given time after the onset of nuclear interphase. The data are from MS2 movies of *hb-MS2ΔZelda* reporter expression in wild-type embryos. Data are shown for each of the 4 individual embryos (color lines in left panel) and pulled (dashed blue line with error bars in the right panel). Also shown is in the transcription pattern extracted from FISH (dashed black line with error bars) from (15).
(AVI)

Acknowledgments

The authors thank Patricia Le Baccon, Mickael Garnier and the Imaging Facility PICT-IBiSA of the Institut Curie, BestGene Inc for transgenics and C. Rushlow and the Bloomington stock center for fly stocks.

Author Contributions

Conceptualization: Tanguy Lucas, Huy Tran, Cécile Fradin, Mathieu Coppey, Aleksandra M. Walczak, Nathalie Dostatni.

Data curation: Tanguy Lucas, Huy Tran, Carmina Angelica Perez Romero, Mathieu Coppey, Aleksandra M. Walczak.

Formal analysis: Tanguy Lucas, Huy Tran, Mathieu Coppey, Aleksandra M. Walczak.

Funding acquisition: Cécile Fradin, Mathieu Coppey, Aleksandra M. Walczak, Nathalie Dostatni.

Investigation: Tanguy Lucas, Huy Tran, Aurélien Guillou, Cécile Fradin, Aleksandra M. Walczak, Nathalie Dostatni.

Methodology: Tanguy Lucas, Huy Tran, Carmina Angelica Perez Romero, Aurélien Guillou, Cécile Fradin, Mathieu Coppey, Nathalie Dostatni.

Project administration: Cécile Fradin, Mathieu Coppey, Aleksandra M. Walczak, Nathalie Dostatni.

Resources: Tanguy Lucas, Huy Tran, Carmina Angelica Perez Romero, Aurélien Guillou.

Software: Huy Tran, Carmina Angelica Perez Romero, Aleksandra M. Walczak.

Supervision: Cécile Fradin, Mathieu Coppey, Aleksandra M. Walczak, Nathalie Dostatni.

Validation: Tanguy Lucas, Huy Tran, Carmina Angelica Perez Romero, Cécile Fradin, Mathieu Coppey, Aleksandra M. Walczak, Nathalie Dostatni.

Visualization: Tanguy Lucas, Huy Tran, Carmina Angelica Perez Romero, Cécile Fradin, Mathieu Coppey, Aleksandra M. Walczak, Nathalie Dostatni.

Writing – original draft: Tanguy Lucas, Huy Tran, Carmina Angelica Perez Romero, Cécile Fradin, Mathieu Coppey, Aleksandra M. Walczak, Nathalie Dostatni.

Writing – review & editing: Tanguy Lucas, Huy Tran, Carmina Angelica Perez Romero, Cécile Fradin, Mathieu Coppey, Aleksandra M. Walczak, Nathalie Dostatni.

References

1. Rogers KW, Schier AF. Morphogen gradients: from generation to interpretation. Annu Rev Cell Dev Biol. 2011; 27:377–407. https://doi.org/10.1146/annurev-cellbio-092910-154148 PMID: 21801015
2. Stathopoulos A, Iber D. Studies of morphogens: keep calm and carry on. Development. 2013; 140 (20):4119–24. https://doi.org/10.1242/dev.095141 PMID: 24086076
3. Porcher A, Dostatni N. The Bicoid morphogen system. Current Biology 2010; 20(5):R249–R54. https://doi.org/10.1016/j.cub.2010.01.026 PMID: 20219179
4. Driever W, Nusslein-Volhard C. A gradient of bicoid protein in Drosophila embryos. Cell. 1988; 54 (1):83–93. PMID: 3383244
5. Abu-Arish A, Porcher A, Czerwonka A, Dostatni N, Fradin C. Fast mobility of Bicoid captured by flourescent correlation spectroscopy: implication for the rapid establishment of its gradient Biophysical Journal. 2010; 99:L33–L5. https://doi.org/10.1016/j.bpj.2010.05.031 PMID: 20712981
6. Gregor T, Wieschaus EF, McGregor AP, Bialek W, Tank DW. Stability and Nuclear Dynamics of the Bicoid Morphogen Gradient. Cell. 2007; 130(1):141–52. https://doi.org/10.1016/j.cell.2007.05.026 PMID: 17632061
7. Chen H, Xu Z, Mei C, Yu D, Small S. A System of Repressor Gradients Spatially Organizes the Boundaries of Bicoid-Dependent Target Genes. Cell. 2012; 149(3):618–29. https://doi.org/10.1016/j.cell.2012.03.018 PMID: 22541432
8. Driever W, Nusslein-Volhard C. The bicoid protein is a positive regulator of hunchback transcription in the early Drosophila embryo. Nature. 1989; 337(6203):138–43. https://doi.org/10.1038/337138a0 PMID: 2911348
9. Struhl G, Struhl K, Macdonald PM. The gradient morphogen bicoid is a concentration-dependent transcriptional activator. Cell. 1989; 57(7):1259–73. PMID: 2567637
10. Crauk O, Dostatni N. Bicoid Determines Sharp and Precise Target Gene Expression in the Drosophila Embryo. Current Biology. 2005; 15(21):1888–98. https://doi.org/10.1016/j.cub.2005.09.046 PMID: 16271865
11. Ronchi E, Treisman J, Dostatni N, Struhl G, Desplan C. Down-regulation of the Drosophila morphogen bicoid by the torso receptor-mediated signal transduction cascade. Cell. 1993; 74(2):347–55. PMID: 8343961

12. Simpson-Brose M, Treisman J, Desplan C. Synergy between the hunchback and bicoid morphogens is required for anterior patterning in Drosophila. Cell. 1994; 78(5):855–65. PMID: 8087852

13. Driever W, Nüsslein-Volhard C. The bicoid protein determines position in the Drosophila embryo in a concentration-dependent manner. Cell. 1988; 54(1):95–104. PMID: 3383245

14. Wolpert L. Positional information and the spatial pattern of cellular differentiation. Journal of Theoretical Biology. 1969; 25(1):1–47. PMID: 4390734

15. Porcher A, Abu-Arish A, Huart S, Roelens B, Fradin C, Dostatni N. The time to measure positional information: maternal Hunchback is required for the synchrony of the Bicoid transcriptional response at the onset of zygotic transcription. Development. 2010; 137(16):2795–804. https://doi.org/10.1242/dev.051300 PMID: 20663819

16. Margolis JS, Borowsky ML, Steingrimsson E, Shim CW, Lengyel JA, Posakony JW. Posterior stripe expression of hunchback is driven from two promoters by a common enhancer element. Development. 1995; 121(9):3067–77. PMID: 7555732

17. Wimmer EA, Carleton A, Harjes P, Turner T, Desplan C. Bicoid-independent formation of thoracic segments in Drosophila. Science. 2000; 287(5462):2476–9. PMID: 10741965

18. Kambadur R, Koizumi K, Stivers C, Nagle J, Poole SJ, Odenwald WF. Regulation of POU genes by castor and hunchback establishes layered compartments in the Drosophila CNS. Genes & development. 1998; 12(2):246–60.

19. Schroder C, Tautz D, Seifert E, Jackle H. Differential regulation of the two transcripts from the Drosophila gap segmentation gene hunchback. The EMBO journal. 1988; 7(9):2881–7. PMID: 2846287

20. Perry MW, Boettiger AN, Levine M. Multiple enhancers ensure precision of gap gene-expression patterns in the Drosophila embryo. Proceedings of the National Academy of Sciences. 2011; 108 (33):13570–5.

21. Perry Michael W, Bothma Jacques P, Luu Ryan D, Levine M. Precision of Hunchback Expression in the Drosophila Embryo. Current Biology. 2012; 22(23):2247–52. https://doi.org/10.1016/j.cub.2012.09.051 PMID: 23122844

22. Raser JM, O'Shea EK. Noise in Gene Expression: Origins, Consequences, and Control. Science. 2005; 309(5743):2010–3. https://doi.org/10.1126/science.1105891 PMID: 16179466

23. Datta RR, Ling J, Kurland J, Ren X, Xu Z, Yucel G, et al. A feed-forward relay integrates the regulatory activities of Bicoid and Orthodenticle via sequential binding to suboptimal sites. Genes & development. 2018; 32(9–10):723–36.

24. Manu Surkova S, Spirov AV, Gursky VV, Janssens H, Kim A-R, et al. Canalization of Gene Expression in the *Drosophila* Blastoderm by Gap Gene Cross Regulation. PLoS Biol. 2009; 7(3):e1000049. https://doi.org/10.1371/journal.pbio.1000049 PMID: 19750121

25. Ochoa-Espinosa A, Yu D, Tsirigos A, Struffi P, Small S. Anterior-posterior positional information in the absence of a strong Bicoid gradient. Proceedings of the National Academy of Sciences of the United States of America. 2009; 106(10):3823–8. https://doi.org/10.1073/pnas.0807878105 PMID: 19237583

26. Lucas T, Ferraro T, Roelens B, De Las Heras Chanes J, Walczak A, Coppey M, et al. Live imaging of Bicoid-dependent transcription in Drosophila embryos Current Biology. 2013; 23(21):2135–9. https://doi.org/10.1016/j.cub.2013.08.053 PMID: 24139736

27. Bertrand E, Chartrand P, Schaefer M, Shenoy SM, Singer RH, Long RM. Localization of ASH1 mRNA Particles in Living Yeast. Molecular Cell. 1998; 2(4):437–45. PMID: 9809065

28. Ferraro T, Lucas T, Clemot M, De Las Heras Chanes J, Desponds J, Coppey M, et al. New methods to image transcription in living fly embryos: the insights so far, and the prospects. Wiley Interdisciplinary REviews Developmental Biology. 2016; 5(3):296–310. https://doi.org/10.1002/wdev.221 PMID: 26894441

29. Estrada J, Wong F, DePace A, Gunawardena J. Information Integration and Energy Expenditure in Gene Regulation. Cell. 2016; 166(1):234–44. https://doi.org/10.1016/j.cell.2016.06.012 PMID: 27368104

30. Fusco D, Accornero N, Lavoie B, Shenoy SM, Blanchard J-M, Singer RH, et al. Single mRNA Molecules Demonstrate Probabilistic Movement in Living Mammalian Cells. Current biology: CB. 2003; 13(2):161–7. PMID: 12546792

31. Blythe Shelby A, Wieschaus Eric F. Zygotic Genome Activation Triggers the DNA Replication Checkpoint at the Midblastula Transition. Cell. 2015; 160(6):1169–81. https://doi.org/10.1016/j.cell.2015.01.050 PMID: 25748651

32. Liang H-L, Nien C-Y, Liu H-Y, Metzstein MM, Kirov N, Rushlow C. The zinc-finger protein Zelda is a key activator of the early zygotic genome in Drosophila. Nature. 2008; 456(7220):400–3. https://doi.org/10.1038/nature07388 PMID: 18931655

33. Bothma JP, Garcia HG, Ng S, Perry MW, Gregor T, Levine M. Enhancer additivity and non-additivity are determined by enhancer strength in the Drosophila embryo. eLife. 2015; 4:e07956.

34. Nien CY, Liang HL, Butcher S, Sun Y, Fu S, Gocha T, et al. Temporal coordination of gene networks by Zelda in the early Drosophila embryo. PLoS Genet. 2011; 7(10):e1002339. https://doi.org/10.1371/journal.pgen.1002339 PMID: 22028675

35. ten Bosch JR, Benavides JA, Cline TW. The TAGteam DNA motif controls the timing of Drosophila pre-blastoderm transcription. Development. 2006; 133(10):1967–77. https://doi.org/10.1242/dev.02373 PMID: 16624855

36. Lopes FJP, Spirov AV, Bisch PM. The role of Bicoid cooperative binding in the patterning of sharp borders in Drosophila melanogaster. Developmental Biology. 2012; 370(2):165–72. https://doi.org/10.1016/j.ydbio.2012.07.020 PMID: 22841642

37. Tran H, Desponds J, Perez Romero CA, Coppey M, Fradin C, Dostatni N, et al. Precision in a rush: trade-offs between positioning and steepness of the hunchback expression pattern. PLoS Computational Biology. In press.

38. Coulon A, Ferguson ML, de Turris V, Palangat M, Chow CC, Larson DR. Kinetic competition during the transcription cycle results in stochastic RNA processing. eLife. 2014; 3:e03939.

39. Gregor T, Tank DW, Wieschaus EF, Bialek W. Probing the Limits to Positional Information. Cell. 2007; 130(1):153–64. https://doi.org/10.1016/j.cell.2007.05.025 PMID: 17632062

40. Desponds J, Tran H, Ferraro T, Lucas T, Perez Romero C, Guillou A, et al. Precision of Readout at the hunchback Gene: Analyzing Short Transcription Time Traces in Living Fly Embryos. PLOS Computational Biology. 2016; 12(12):e1005256. https://doi.org/10.1371/journal.pcbi.1005256 PMID: 27942043

41. Juven-Gershon T, Hsu J-Y, Kadonaga JT. Caudal, a key developmental regulator, is a DPE-specific transcriptional factor. Genes & development. 2008; 22(20):2823–30.

42. Berg HC, Purcell EM. Physics of chemoreception. Biophysical Journal. 1977; 20(2):193–219. https://doi.org/10.1016/S0006-3495(77)85544-6 PMID: 911982

43. Bialek W, Setayeshgar S. Physical limits to biochemical signaling. PNAS. 2005; 102(29):10040–5. https://doi.org/10.1073/pnas.0504321102 PMID: 16006514

44. Kaizu K, de Ronde W, Paijmans J, Takahashi K, Tostevin F, ten Wolde Pieter R. The Berg-Purcell Limit Revisited. Biophysical Journal. 2014; 106(4):976–85. https://doi.org/10.1016/j.bpj.2013.12.030 PMID: 24560000

45. Tran H, Desponds J, Perez-Romero CA, Coppey M, Fradin C, Dostatni N, et al. Precision in a rush: hunchback pattern formation in a limited time. To be submitted and deposited on the Bioarxiv shortly. in prep.

46. Slutsky M, Mirny LA. Kinetics of Protein-DNA Interaction: Facilitated Target Location in Sequence-Dependent Potential. Biophysical Journal. 2004; 87(6):4021–35. https://doi.org/10.1529/biophysj.104.050765 PMID: 15465864

47. Fradin C. On the importance of protein diffusion in biological systems: The example of the Bicoid morphogen gradient. Biochimica et Biophysica Acta (BBA)—Proteins and Proteomics. 2017; 1865(11, Part B):1676–86.

48. Mir M, Reimer A, Haines JE, Li X-Y, Stadler M, Garcia H, et al. Dense Bicoid hubs accentuate binding along the morphogen gradient. Genes & Development. 2017; 31(17):1784–94.

49. Xu H, Sepúlveda LA, Figard L, Sokac AM, Golding I. Combining protein and mRNA quantification to decipher transcriptional regulation. Nature Methods. 2015; 12:739. https://doi.org/10.1038/nmeth.3446 PMID: 26098021

50. Chou T-b, Perrimon N. The Autosomal FLP-DFS Technique for Generating Germline Mosaics in Drosophila melanogaster. Genetics. 1996; 144(4):1673–9. PMID: 8978054

51. Venken KJT, Carlson JW, Schulze KL, Pan H, He Y, Spokony R, et al. Versatile P[acman] BAC libraries for transgenesis studies in Drosophila melanogaster. Nat Meth. 2009; 6(6):431–4.

52. Warming S, Costantino N, Court DL, Jenkins NA, Copeland NG. Simple and highly efficient BAC recombineering using galK selection. Nucleic Acids Research. 2005; 33(4):e36–e. https://doi.org/10.1093/nar/gni035 PMID: 15731329

53. Perez-Romero CA, Tran H, Coppey M, Walczak AM, Fradin C, Dostatni N. Live imaging of mRNA transcription in Drosophila Embryos. Methods Mol Biol. In press; "Morphogen Gradients: Methods and Protocols" edited by J. Dubrulle.

54. Tran H, Perez-Romero CA, Ferraro T, Fradin C, Dostatni N, Coppey M, et al. LiveFly—a toolbox for the analysis of transcription dynamics in live Drosophila embryos. Methods Mol Biol. In press;"Morphogen Gradients: Methods and Protocols" edited by J. Dubrulle.

55. Gunawardena J. A linear framework for time-scale separation in nonlinear biochemical systems. PloS one. 2012; 7(5):e36321. https://doi.org/10.1371/journal.pone.0036321 PMID: 22606254

56. Lloyd-Price J, Gupta A, Ribeiro AS. SGNS2: a compartmentalized stochastic chemical kinetics simulator for dynamic cell populations. Bioinformatics (Oxford, England). 2012; 28(22):3004–5.